Unibody microscope objective tipped with a microsphere: design, fabrication, and application in subwavelength imaging

Yan, Bing; Song, Yang; Yang, Xibin; Xiong, Daxi; Wang, James

Applied Optics

DOI:
10.1364/AO.386504

Published: 10/03/2020

Peer reviewed version

Unibody microscope objective tipped with a microsphere: design, fabrication, and application in subwavelength imaging

Bing Yan,[1,2] Yang Song,[2] Xibin Yang,[2,3] Daxi Xiong,[2] and Zengbo Wang[1,*]

[1]School of Computer Science and Electronic Engineering, Bangor University, Dean Street, Bangor, Gwynedd LL57 1UT, UK
[2]Center of Optics Health, Suzhou Institute of Biomedical Engineering and Technology, Chinese Academy of Sciences, No. 88 Keling Street, Suzhou, Jiangsu 215163, China
[3]e-mail: yangxb@sibet.ac.cn
*Corresponding author: z.wang@bangor.ac.uk

Microsphere-based subwavelength imaging technique was first demonstrated in 2011. After nearly a decade of efforts, such technique has spawned numerous interests in fields such as laser nano-machining, imaging, sensing, and biological detection. For wider industrial-scale application of the technique, a robust and low-cost objective lens incorporating a microsphere lens is highly desired and sought by many researchers. In this work, we demonstrate a unibody microscope objective lens formed by tipping a high-index microsphere onto a plano-convex lens and subsequently fitting them into a conventional objective lens. We call this the plano-convex-microsphere (PCM) objective, which resembles the appearance and operation of an ordinary microscope objective while providing super-resolving power in discerning subwavelength 100 nm features ($\lambda/4.7$) in air and far-field conditions. The imaging performance of the PCM objective, along with the working distance, has been systematically investigated. It has a calibrated resolution of $\lambda/3$ in the far field, a numerical aperture of 1.57, and a working distance of 3.5 μm. With the assistance of a scanning process, larger-area imaging is realized. The PCM objective can be easily adapted to existing microscope systems and is appealing for commercialization.

1. INTRODUCTION

With the advancement of life science and nano-technology, research has urgent need for novel instruments to achieve nanoscale observation, which has also prompted a revolution of optical microscopy. One of the great challenges in optical imaging is to break the diffraction limit, which was formulated as $d = \lambda/2\mathrm{NA}$ (d is minimum resolvable distance, λ is the wavelength of light, NA is the numerical aperture of the objective) [1]. In 1984, the development of near-field scanning optical microscopy (NSOM), which introduced the near-field method of collecting evanescent waves by a physical probe with a subwavelength aperture positioned close to an object's surface opened a new door for super-resolution research [2]. In recent years, owing to the rise of metamaterials, nanophotonics, and plasmonics, we have witnessed a number of exciting developments in super-resolution imaging, including, for example, super-resolution fluorescent microscopy [3–5], negative-index metamaterial superlenses [6,7], super-oscillation lenses [8], time-reversal imaging [9], the Maxwell fisheye [10], the scattering lens [11] and the cascaded plasmonic superlens [12]. However, they fail to operate or have deteriorated performance under white-light illumination. Recently, it was discovered that dielectric spherical and cylindrical lenses with microscale diameter can surpass the diffraction barrier through a phenomenon known as a "photonic nanojet" [13,14], which was extended to other shapes including conical and cuboid microlenses [15,16]. The photonic nanojet has been proven to be a simple and superior way to achieve a resolution of $\sim\lambda/6$ to $\sim\lambda/8$ in white-light conditions [17,18]. The super-resolution capability can be explained by efficient collection and conversion of the high spatial harmonics of the evanescent waves of the underlying object in the near-field zone. Unlike other super-resolution techniques, the microsphere superlens provides a real-time visualization under white-light illumination; meanwhile, it is label free and has low intrinsic loss at higher optical frequency. These unique features have attracted a number of groups across the world for further development. For instance, incorporation of a high-index microsphere into flexible elastomers was reported to improve its durability and reusability for observations at a specific position [19,20]. The microsphere was coupled with

a confocal microscope to improve the maximal resolvability to the sub-50 nm scale [21–23]. Furthermore, microlens nanoscopes in extraordinary forms were also demonstrated, such as nanoparticle-based metamaterial hemisphere superlenses leading to white lighting of 45 nm resolution [24] and biological superlenses using spider silks and cells [25,26].

Although research has revealed the capability of super-resolution for microsphere-based superlenses, the imaging field of view (FOV) is often very small, typically only a quarter of microsphere's diameter, which is an inevitable issue in practical use. Efforts have been made recently to circumvent such problem. Our previous work presented in 2017 provided a simple but efficient approach to adapt the microsphere lens in an ordinary microscope. With a 3D-printed objective adaptor, the microsphere can work synchronously under the objective to realize large-area scanning imaging [27]. Similar work was also demonstrated in Yang's previous paper [28]. However, due to lack of feedback mechanisms, these lenses are still in contact with samples or require lubricants to reduce the friction during scanning, which adds invasiveness to sensitive specimens. In addition, the optical trapping method was reported to control the microsphere; however, this method was limited to a liquid environment [29]. The most effective method among the previously published research is the manipulation of a single microsphere lens by tip-based scanning techniques [30–32]. In 2016, Wang *et al.* bonded a barium titanium glass (BTG) microsphere onto an atomic force microscope (AFM) tip; with the advantage of precise positioning and feedback monitoring, the system has high precision in maintaining the distance between the microsphere and objects. Therefore, samples possessing surfaces of different roughnesses can be either super-resolved by contact or constant-working-distance scanning mode [31]. Nevertheless, this technique involves sophisticated and a pricey near-field tip control system, which requires professional skill to operate. Also, their work has been limited to use in a liquid environment. We aim to develop a low-cost, easy-to-implement, and universal microsphere-based super-resolution scanning imaging system for noninvasive nano-imaging that is suitable for both air and liquid environments.

In this work, we employed a new design where the microsphere lens is a compound part consisting of a plano-convex lens and a microsphere lens (in short, "PCM"), which can perform as an individual optical probe and is able to be perfectly fitted onto an ordinary objective lens to form a unibody PCM-objective lens. The unibody superlens has the same appearance and simple operation as an ordinary microscope objective but also provides noninvasive real-time super-resolving capability in air conditions. Its imaging performance was evaluated along with the working distance. Meanwhile, with the assistance of a high-resolution nano-stage, large-area scanning imaging was realized. Furthermore, the focusing properties of the PCM lens were theoretically investigated. This unibody PCM-objective design is highly versatile, meaning that existing optical microscope systems can be converted to super-resolution nanoscopes by simply installing our lens. The work has raised the usability of the microsphere-based superlens technique to a new level.

2. PREPARATION OF UNIBODY PCM OBJECTIVE

In this paper, a unibody PCM objective is presented in the form of combination of a plano-convex microsphere lens and an ordinary microscope objective. As previously reported, the PCM lens has the advantages of excellent reliability and usability, and it can generate a sub-diffraction photonic nanojet in air conditions, which can be used as a low-cost and simple technique for laser nano-patterning [33]. Here we introduce the PCM lens to imaging application through integrating it into an optical microscope objective. As Fig. 1(a) illustrates, BTG microspheres ($n_p = 1.9$) with diameters of 25, 38, and 50 μm were aligned and attached onto polydimethylsiloxane (PDMS, SYLGARD 184, DOW CORNING, $n_m = 1.4$, with stable optical properties under experimental conditions), which was pre-coated (spin-coating at 2000 rpm for 1 minute)

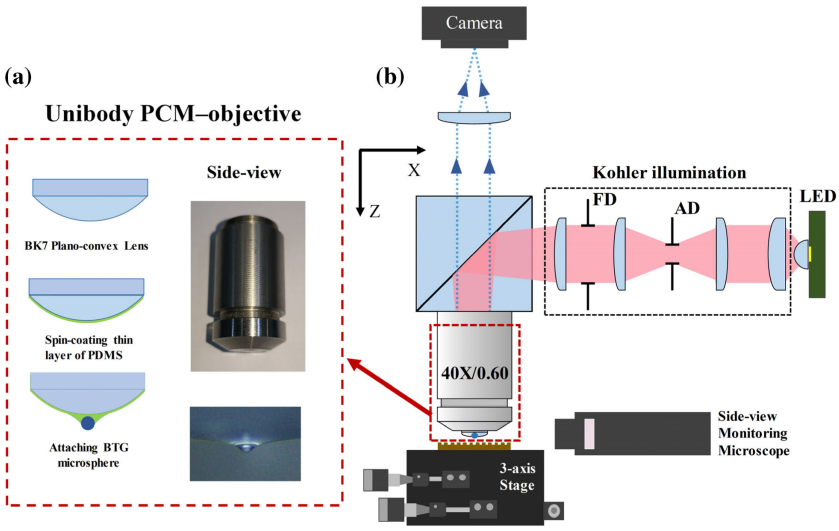

Fig. 1. Schematic of unibody PCM-objective imaging system. (a) Preparation of PCM lens and installation of unibody PCM objective. (b) Self-developed imaging system.

onto a spherical crown of a BK7 plano-convex lens (LA1700, Thorlabs, radius of curvature: 15.5 mm; diameter: 6 mm; thickness: 1.8 mm; focal length: 30 mm). Due to the capillary force, once the BTG microspheres came in contact with the edge of the liquid PDMS, they were pulled and immersed into the PDMS layer to form a partial encapsulation of the BTG microspheres. The depth of encapsulation may vary slightly during the process, which is not critical to imaging performance when the depth is between 20% and 100% of the particle diameter as shown later by experiments and simulation. The PDMS was then solidified by heating at 90°C for 15 minutes. This resulted in the formation of a probe-like plano-convex microsphere (PCM) lens, where a single microsphere slightly extruded out. Afterwards, the PCM lens was attached onto a custom-designed adjustable objective adapter. The adapter consists of two metal components; the upper part is fixed to the objective (40 × 0.6NA), and the lower part holds the PCM lens. These two components are fitted together with a threaded connection, and hence the distance between the PCM lens and the objective is adjustable by manual rotation. Then the PCM objective was installed onto a self-built imaging system as shown in Fig. 1(b). A blue LED light source (central wavelength 470 nm, bandwidth 24 nm) is incident through the Kohler arrangement with an aperture diaphragm (AD) and field diaphragm (FD), which can contribute to achieving better image contrast. In our experiments, the PCM objective was kept static, and the sample was pinpointed by moving the underlying stage. The movement of the sample was performed using a high-resolution nano-stage (Nanomotor SNM01, Shinopto), with 20 nm resolution in the $x-y-z$ direction and a travel range of 25.4 mm. In order to avoid damage to the PCM lens and sample during focus adjustment, a long-focal-length zoom lens was placed horizontally at the side for monitoring the gap between the microsphere bottom and the top of the sample. The exact working distance (WD) can be known by measuring the travel distance in the z direction of the nano-stage from the working plane towards the lens boundary. Once the sample is touching the lens, a slight pressure causes deformation of the image, which determines the contact state.

3. RESULTS AND DISCUSSION

A. Investigation of Imaging Performance

Near-field imaging requires a WD within wavelength scale or even in contact. However, it is invasive and may bring limitations in imaging of sensitive specimens, for instance, biological samples. Therefore, a contactless process is essential to avoid polluting and damaging specimens. In this experiment, we evaluated the imaging performance, including magnification and resolvability of the developed unibody PCM objective, at different WDs. The experiment was carried out by using a sample of integrated chip (IC) chip with features of 400 nm blocks and 200 nm intervals as shown in Fig. 2(a). Figure 2(b) indicates the image obtained using a bare objective (40 × NA0.60), which has a theoretical resolution limit of 390 nm ($\lambda/2$NA). As the minimum feature size is beyond the resolvability of the objective, it gave a blurry image and detail information was lost. In order to evaluate the imaging enhancement of the PCM lens, we kept all conditions (objective, illumination, and camera) the same and only installed PCM lenses of different diameters. Since the sample was placed within the focal length of the bottom PCM lens, the top objective picked up the magnified virtual image generated by the PCM lens. Figures 2(d)–2(f) illustrate the magnifications of the images obtained by the microspheres of 25, 38, and 52 μm when the WD increases from zero, respectively. As shown, the features of 200 nm separations can be clearly resolved through the contribution of the PCM lens; meanwhile, the magnification ascends along with increasing distance, which is similar behavior to geometrical optics. This implies that the PCM lens not only has the features of a classical lens but also contributes significantly to enhancing the resolution. Furthermore, the comparison between three sizes of microspheres also reveals that the PCM lens with a smaller microsphere exhibits greater magnification factor at the same WD, which is summarized in Fig. 2(c). It is worth noting that the imaging pincushion distortion appeared obviously when the lens was adjacent to the object. This phenomenon was gradually suppressed by increasing the WD. For example, in case of contact (WD = 0), it is clear that the small area in the central region has better resolution and contrast than the periphery of the microsphere; concurrently a radial increment of the magnification factor results in a distorted image as shown in Figs. 2(d)i, 2(e)i, 2(f)i. This heterogeneous imaging performance may be due to the aberration of geometric construction of the spherical lens. With the lens moving away from the object, the uneven imaging performance and distortion is gradually suppressed, but the contrast and FOV are reduced correspondingly. Therefore, there is a compromise between image quality and magnification factor, and it is necessary to make a trade-off to get the most balanced performance.

In addition, smaller sized samples were used to further investigate the super-resolution ability of the designed unibody PCM objective. Here we used a 38 μm microsphere PCM lens to capture a Blu-ray disc with features of 200 nm stripes and 100 nm grooves [Fig. 3(a)] at different WDs. It may be hard to resolve these patterns by standard illumination settings. However, using oblique illumination with an incident angle roughly between 10 and 40 deg and partial illumination would produce an enhancement in image quality. This was realized by adjustment of the AD and FD. These illumination conditions for improving imaging performance were also discovered and proved experimentally and theoretically by our previous paper and the work of other groups [25,27,31]. According to the results demonstrated and discussed in Fig. 2(e), the imaging performance was better balanced with a WD range of 1 to 3.5 μm. Therefore, the Blu-ray disc imaging experiment was carried out within a corresponding WD range. As can be seen at 1.3 μm WD [Fig. 3(b)], the imaging zone under the microsphere was partially illuminated with a shadow at one side. Even though the 100 nm features can be resolved, the overall image quality was affected by the difference in illumination between the center and outer region of the microsphere. Due to inclined and partial illumination, the brightness distribution of the image is uneven, especially in the shorter WD. This brightness difference was gradually improved with an increased in WD. At a WD of around 3 μm [Figs. 3(e) and 3(f)], the image exposure became more equalized. The features of the Blu-ray disc can be clearly distinguished with magnification factor of

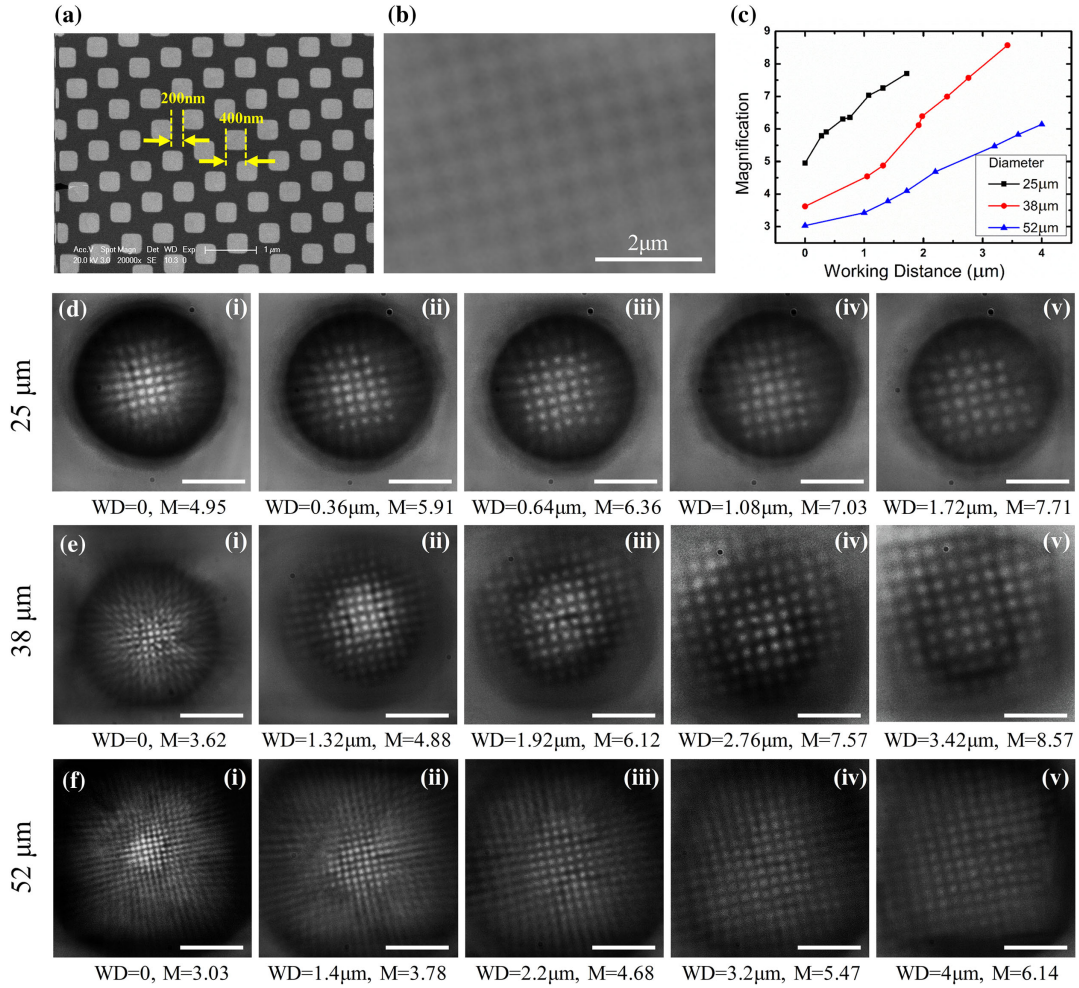

Fig. 2. Investigation of magnifications (M) of the PCM lens from different working distances (WDs). (a) SEM image of IC chip with 400 nm blocks and 200 nm intervals. (b) IC chip image taken by optical objective (40X, 0.6 N.A.). (c) Curve of magnification of three sizes of microspheres with WDs. (d)–(f) PCM lens with 25, 38, and 52 μm BTG microspheres embedded. Magnifications (M) of each size lens were evaluated by different WDs. The scale bar in (b) is 2 μm and in (d)–(f) is 20 μm.

∼ 8. After 4 μm, images turned misty and lost details [Figs. 3(h) and 3(i)]. It was observed that the WD of ∼ 4 μm is a critical experimental value, above which super-resolution is no longer possible.

B. Scanning Imaging

The above-mentioned results have verified the imaging performance of the developed unibody PCM objective, where the super-resolving ability is mainly determined by the PCM lens within certain WD ranges, even though the FOV for super-resolution is limited to the central part of the microsphere. To expand the viewable area, scanning imaging is necessary. In our unibody PCM objective, the PCM lens is synchronized with an objective lens. During the scanning operation, it is beneficial to keep the position of both parts of the lens constant. Different from our previous work [27], the unibody PCM objective operates in air; it is now friction free and no lubricant media between lens and object is needed. Due to the elimination of the dragging issue, we can easily and precisely move the sample to the designated location with knowing its relative coordinates. Therefore, image stitching becomes easier. In this study, scanning imaging was performed with a well-structured semiconductor IC chip and Blu-ray disc sample to demonstrate the feasibility of scanning imaging using the developed unibody PCM objective as shown in Fig. 4. The IC chip in Fig. 4(a) is the same as used in Fig. 2, and it has features of 200 nm and 400 nm and was imaged by 38 μm microsphere with WD around 2.8 μm. Then the sample was moved in the $X - Y$ plane and kept constant in the Z direction to get the same quality image in every location. The scanning path followed line-by-line scanning, as shown by the yellow dash line in Fig. 4(b). The camera captured one frame for every 1.2 μm the stage travelled, and totally 10 × 10 frames were recorded. Large-area imaging can be achieved by stitching together those 100 recorded frames, and the finalized image is demonstrated in Fig. 4(b). Similar scanning experiments were also performed on a Blu-ray disc sample [Figs. 4(c) and 4(d)] and more complex structures of the IC chip [Figs. 4(e) and 4(f)]. The scanning processes were video recorded (Visualization 1, Visualization 2, and Visualization 3).

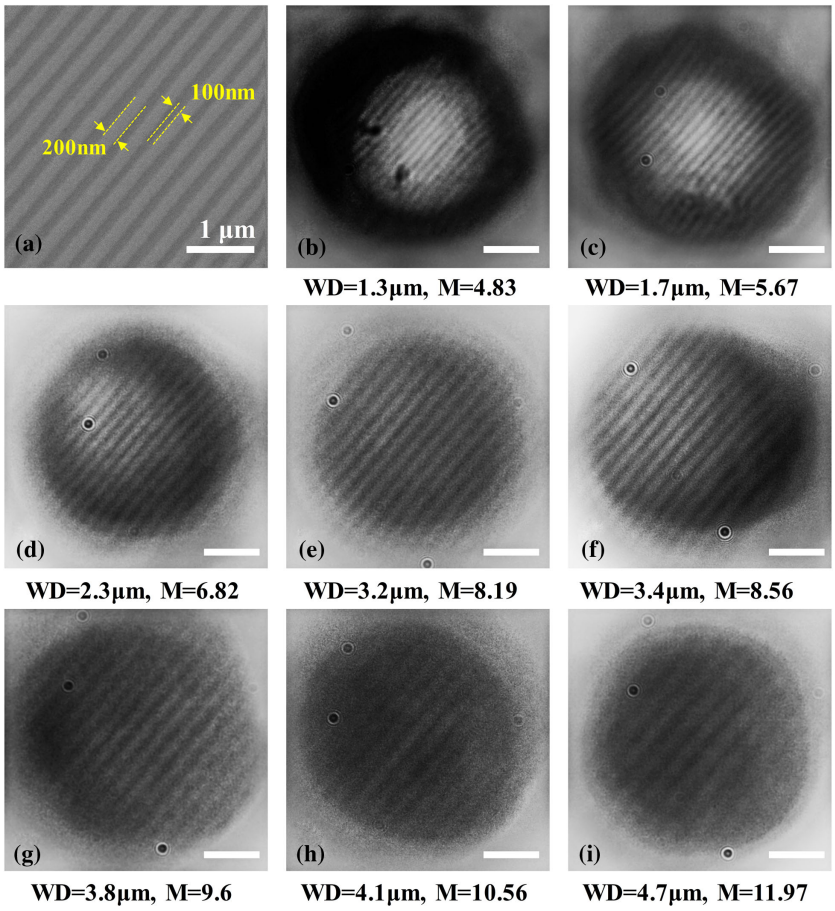

Fig. 3. Investigation of resolvability of the PCM lens from different WDs. (a) SEM image of a Blu-ray disc with 200 nm strips and 100 nm grooves. (b)–(i) Blu-ray disc image taken by the PCM lens with 38 μm BTG microspheres embedded at different WDs. The scale bar in (a) is 1 μm and in (b)–(i) is 10 μm.

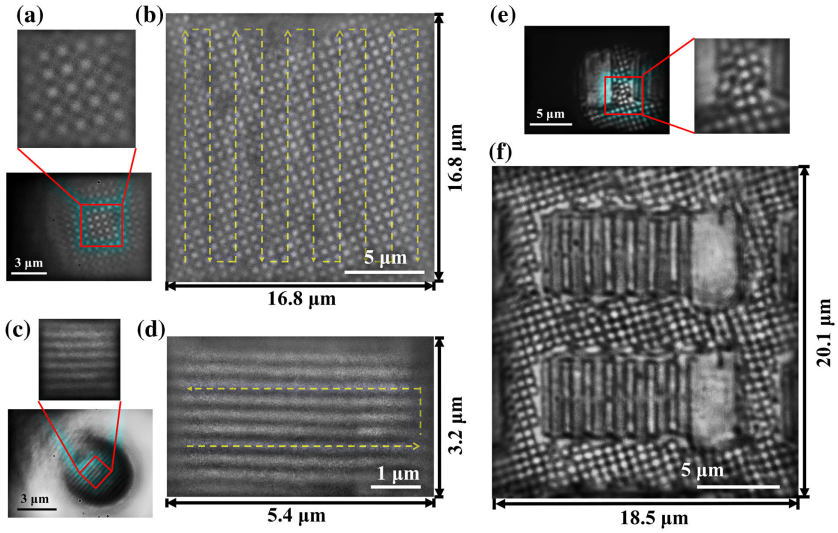

Fig. 4. Scanning super-resolution imaging and image stitching. (a) Single frame image of IC chip sample. (b) Stitched image of 10 × 10 frames. (c) Single frame image of the Blu-ray disc. (d) Stitched image of 20 × 2 frames. (e) Single frame image of complex structure of the IC chip. (f) Stitched image of 13 × 10 frames.

C. Theoretical Analysis

The size of the BTG microsphere can influence the resolution, which has been discussed in Refs. [13,17,20]. Typically, smaller size can contribute to a better resolution. However, its focal length tends to be shorter, which make the super-resolution effect happen in the near-field zone or even in contact conditions. Therefore, noninvasive nano-imaging would be difficult to achieve by a smaller microsphere. Generating large-area scanning images requires smooth and accurate scanning, which means that maintaining a gap between the microsphere and the sample is essential for avoiding lens–sample friction and unintentional scratches on delicate samples. For such consideration, we have chosen a BTG microsphere with diameter from 25–60 μm to provide a reasonable balance between WD and resolution.

In the experiment, we found that the encapsulated status of the microsphere by the PDMS might be slightly varied due to microsphere size, the thickness of the PDMS layer, and process deviation. To further investigate whether this deviation would affect imaging performance and to understand the focusing characteristics of the PCM lens in different capped cases, computational modeling was performed using in-house developed code based on a hybrid finite element and physical optics method. Since the curvature radius of the plano-convex lens is 15.5 mm, which is much greater than the size of the microsphere, the curved surface can be regarded as a plane surface in the simulation range. A plane wave (470 nm) with x polarization was set to propagate through a 38 μm BTG microsphere ($n_p = 1.9$) partially encapsulated by a PDMS layer ($n_m = 1.4$) to imitate the PCM lens in the experiment. The computation was performed on a server (Xeon CPU, 28 cores, 256 GB RAM), which takes about 12–16 hours for each parameter setting.

Here comparisons were made between different capsulation conditions, including PDMS immersion ratio from 0% to 100%. Figures 5(a)–5(f) show the calculated optical field distribution in the $y - z$ plane in the respective capsulation cases. In case of a non-immersed BTG microsphere [Fig. 5(a)], the plane wave is focused at the boundary of the shadow side and then quickly diverges. Under this circumstance, although field enhancement can reach over 3500×, a magnified virtual image cannot be generated. When the BTG microsphere begins to submerge in the PDMS, its focus moves into the air region. Figures 5(b)–5(f) reveal that the light wave is converged after passing through the capped particle lenses, and focused hot spots exhibit an elongated shape and then diverge with distance. The maximum intensity is found at locations several micrometers away from the microsphere and quickly drops afterward. As expected, Fig. 5(f) (fully capped case) shows a slightly longer focal spot in the z direction than other cases. Figure 5(g) specifically compares the intensity profiles along the z direction of 11 cases. As observed, differently capped microspheres can immensely enhance light by more than 2500 times and, meanwhile, 20%–90% capped microspheres generate very similar intensity distribution along the z axis. Their highest peaks appear at around $z = 26$ μm (WD = 7 μm) in air. This reveals that varied formations of encapsulation in the range of 20%–90% have a negligible effect on their focal length. In addition, capsulations of 0%–10% produce completely different focusing, either single peak occurring at the boundary. Furthermore, the calculated spot size, full width at half-maximum (FWHM) along the y direction, corresponding to the WD is illustrated in Fig. 5(h). Here we only consider the capsulation case that can generate a virtual image, and 0%–10% capped cases were not considered. In 20%–100% capsulations, the FWHM spot size fluctuates between 150 nm ($\sim \lambda/3$) and 320 nm before the focus, which grows to about 270–350 nm at the focus point ($z = 26$ μm) and then jumps to microscale due to light divergence. At distances less than 23.5 μm (WD < 4.5 μm), the spot sizes in all cases are in the super-resolution regime with resolution between $\lambda/3$ and $\lambda/2$. Outside this range, the sub-diffraction focusing is lost. Moreover, we picked three points in the 80% capped condition to plot a lateral focusing profile. In the three insets presented in Fig. 5(h), the central spot shapes at 19 and 22 μm exhibit non-circular patterns, but smaller widths in the y direction and some peripheral concentric ring patterns are found. A circular hot spot is generated at the focal point ($z = 26$ μm), and surrounding ring patterns are suppressed. As previous experimental results described, imaging performance is affected by the WD, and the super-resolution phenomenon happens within ~ 4 μm WD. This is thus consistent with the presented theoretical simulations. We may draw conclusions from the above simulation results that the formations of microsphere capsulation in the range of 20%–100% have an insignificant effect on focusing performance, including focal length, intensity enhancement, and imaging resolution. This is beneficial for manufacturing PCM lens because subtle process deviation would not result in an obvious discrepancy in imaging performance.

The present PCM objective, with ability to resolve 100 nm features in a far-field setup in the air, is a "modest performance" super-resolution ($\sim \lambda/3$) objective lens that does not deliver as strong super-resolution (typically $\lambda/6$–$\lambda/8$) as other forms of near-field dielectric superlenses (e.g., TiO_2 [24], hybrid nanolens [34]). It is still, however, very unique, and has the clear advantages of performing reliable scanning super-resolution imaging in dry conditions. Thanks to the immersion design, the PCM objective is relatively stable when switching from dry to liquid environments, where resolution is slightly improved but insignificant. The design holds great promise for commercial development. A higher-resolution PCM objective, with the ability to resolve 50–70 nm features in the air with micrometer-scale WD, could be achieved by using high-index TiO_2 microspheres ($n = 2.4$), owing to their stronger light confinement effects. This is currently in progress. A new physical effect—optical super-resonance in microspheres due to high-order Fano resonance—could be another new route to achieve extreme super-resolution in a PCM objective and other microsphere-based techniques, but it will require a new modulated lighting source to match the super-resonance conditions [35,36]. The PCM lens will find many interesting engineering and biomedical applications, including sensing, diagnostics, trapping, manipulation of nano-objects, and laser nano-marking [33]. The PCM lens design concept can be extended to bio-inspired imaging systems (e.g., artificial compound moth eyes based on BTG microspheres) to enable new super-resolution imaging capability to be included in such systems [37–39].

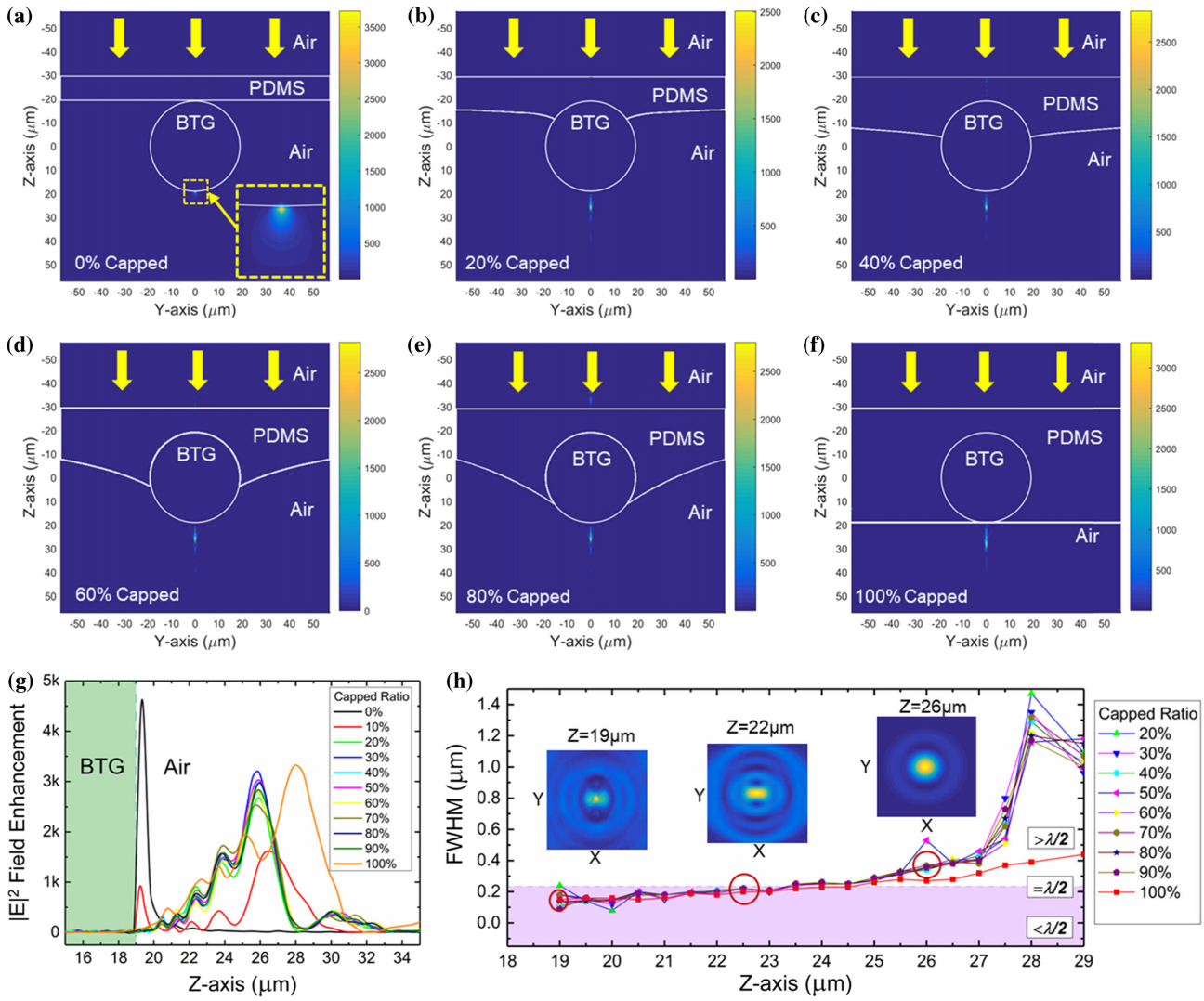

Fig. 5. Modelling of PCM lens focusing properties. $y-z$-plane electric field intensity distribution of 38 μm BTG microspheres encapsulated by PDMS with (a) 0%, (b) 20%, (c) 40%, (d) 60%, (e) 80%, and (f) 100%. (g) Comparison of $|E|^2$ enhancement along the z axis between different capsulation cases. (h) Comparison of FWHM along the y axis between different capsulation cases.

4. CONCLUSION

In summary, we have developed a unibody PCM objective by tactfully integrating a microsphere lens onto an ordinary microscope objective lens. It is advantageous to simplify the imaging system and improve usability in practical operation. The resolution of the developed lens in different WDs was experimentally and theoretically investigated. As the results indicated, 100 nm Blu-ray disc features were discernible in air conditions by a 38 μm microsphere PCM lens within 4 μm WD. Such WD provides a possibility for noninvasive scanning imaging. This lens design is versatile, making it convenient to turn a normal microscope into a super-resolution nanoscope without too much expense. Moreover, it has potential for other super-resolution applications.

Funding. European Regional Development Fund (81400); Royal Society (IEC\NSFC\181378); National Key Research and Development Program of China (2017YFC0109900, 2018YFC0114800); National Natural Science Foundation of China (61405238); Key RD Program of Jiangsu Province, China (BE2018666).

Disclosures. The authors declare no conflicts of interest.

REFERENCES

1. E. Abbe, "Beiträge zur Theorie des Mikroskops und der mikroskopischen Wahrnehmung," Arch. für mikroskopische Anat. **9**, 413–418 (1873).
2. D. W. Pohl, W. Denk, and M. Lanz, "Optical stethoscopy: image recording with resolution λ/20," Appl. Phys. Lett. **44**, 651–653 (1984).
3. S. W. Hell and J. Wichmann, "Breaking the diffraction resolution limit by stimulated emission: stimulated-emission-depletion fluorescence microscopy," Opt. Lett. **19**, 780–782 (1994).
4. E. Betzig, G. H. Patterson, R. Sougrat, O. W. Lindwasser, S. Olenych, J. S. Bonifacino, M. W. Davidson, J. Lippincott-Schwartz, and H. F. Hess, "Imaging intracellular fluorescent proteins at nanometer resolution," Science **313**, 1642–1645 (2006).

5. S. T. Hess, T. P. K. Girirajan, and M. D. Mason, "Ultra-high resolution imaging by fluorescence photoactivation localization microscopy," Biophys. J. **91**, 4258–4272 (2006).
6. X. Zhang and Z. Liu, "Superlenses to overcome the diffraction limit," Nat. Mater. **7**, 435–441 (2008).
7. J. B. Pendry, "Negative refraction makes a perfect lens," Phys. Rev. Lett. **85**, 3966–3969 (2000).
8. E. T. Rogers, J. Lindberg, T. Roy, S. Savo, J. E. Chad, M. R. Dennis, and N. I. Zheludev, "A super-oscillatory lens optical microscope for subwavelength imaging," Nat. Mater. **11**, 432–435 (2012).
9. M. Davy, J. G. Minonzio, J. de Rosny, C. Prada, and M. Fink, "Influence of noise on subwavelength imaging of two close scatterers using time reversal method: theory and experiments," Prog. Electromagn. Res. **98**, 333–358 (2009).
10. O. Bitton, R. Bruch, and U. Leonhardt, "Two-dimensional Maxwell fisheye for integrated optics," Phys. Rev. Appl. **10**, 044059 (2018).
11. J. H. Park, C. Park, Y. H. Cho, and Y. Park, "Scattering super-lens: subwavelength light focusing and imaging via wavefront shaping in complex media," in *Conference on Lasers and Electro-Optics (CLEO)* (2014).
12. H. Li, L. Fu, K. Frenner, and W. Osten, "Cascaded plasmonic superlens for far-field imaging with magnification at visible wavelength," Opt. Express **26**, 10888–10897 (2018).
13. Z. Chen, A. Taflove, and V. Backman, "Photonic nanojet enhancement of backscattering of light by nanoparticles: a potential novel visible-light ultramicroscopy technique," Opt. Express **12**, 1214–1220 (2004).
14. Y. F. Lu, L. Zhang, W. D. Song, Y. W. Zheng, and B. S. Luk'yanchuk, "Laser writing of a subwavelength structure on silicon (100) surfaces with particle-enhanced optical irradiation," J. Exp. Theor. Phys. Lett. **72**, 457–459 (2000).
15. I. V. Minin, O. V. Minin, and Y. E. Geintz, "Localized EM and photonic jets from non-spherical and nonsymmetrical dielectric mesoscale objects: brief review," Ann. Phys. **527**, 491–497 (2015).
16. S. Lecler, S. Perrin, A. Leong-Hoi, and P. Montgomery, "Photonic jet lens," Sci. Rep. **9**, 4725 (2019).
17. Z. Wang, W. Guo, L. Li, B. Luk'yanchuk, A. Khan, Z. Liu, Z. Chen, and M. Hong, "Optical virtual imaging at 50 nm lateral resolution with a white-light nanoscope," Nat. Commun. **2**, 218 (2011).
18. Z. Wang, "Microsphere super-resolution imaging," Nanoscience **3**, 193–210 (2016).
19. A. Darafsheh, N. I. Limberopoulos, J. S. Derov, D. E. Walker, and V. N. Astratov, "Advantages of microsphere-assisted super-resolution imaging technique over solid immersion lens and confocal microscopies," Appl. Phys. Lett. **104**, 061117 (2014).
20. A. Darafsheh, G. F. Walsh, L. Dal Negro, and V. N. Astratov, "Optical super-resolution by high-index liquid-immersed microspheres," Appl. Phys. Lett. **101**, 141128 (2012).
21. Y. Yan, L. Li, C. Feng, W. Guo, S. Lee, and M. H. Hong, "Microsphere coupled scanning laser confocal nanoscope for sub-diffraction-limited imaging at 25 nm lateral resolution in the visible spectrum," ACS Nano **8**, 1809–1816 (2014).
22. B. S. Luk'yanchuk, R. Paniagua-Dominguez, I. Minin, O. Minin, and Z. B. Wang, "Refractive index less than two: photonic nanojetsyesterday, today and tomorrow," Opt. Mater. Express **7**, 1820–1847 (2017).2159-3930
23. Z. B. Wang and B. S. Luk'yanchuk, "Super-resolution imaging and microscopy by dielectric particle-lenses," in *Book Label-Free Super-Resolution Microscopy*, V. Astratov, ed. (Springer, 2019).
24. W. Fan, B. Yan, Z. B. Wang, and L. M. Wu, "Three-dimensional all-dielectric metamaterial solid immersion lens for subwavelength imaging at visible frequencies," Sci. Adv. **2**, e1600901 (2016).
25. J. N. Monks, B. Yan, N. Hawkins, F. Vollrath, and Z. B. Wang, "Spider silk: mother nature's bio-superlens," Nano Lett. **16**, 5842–5845 (2016).
26. Y. Li, X. Liu, and B. Li, "Single-cell biomagnifier for optical nanoscopes and nanotweezers," Light-Sci. Appl. **8**, 61 (2019).
27. B. Yan, Z. B. Wang, A. L. Parker, Y. Lai, P. J. Thomas, L. Yue, and J. N. Monks, "Superlensing microscope objective lens," Appl. Opt. **56**, 3142–3147 (2017).
28. G. Huszka, H. Yang, and M. A. Gijs, "Microsphere-based super-resolution scanning optical microscope," Opt. Express **25**, 15079–15092 (2017).
29. A. Bezryadina, J. Li, J. Zhao, A. Kothambawala, J. Ponsetto, E. Huang, J. Wang, and Z. Liu, "Localized plasmonic structured illumination microscopy with optically trapped microlens," Nanoscale **9**, 14907–14912 (2017).
30. L. A. Krivitsky, J. J. Wang, Z. B. Wang, and B. Luk'yanchuk, "Locomotion of microspheres for super-resolution imaging," Sci. Rep. **3**, 3501 (2013).
31. F. Wang, L. Liu, H. Yu, Y. Wen, P. Yu, Z. Liu, Y. Wang, and W. J. Li, "Scanning superlens microscopy for non-invasive large field-of-view visible light nanoscale imaging," Nat. Commun. **7**, 13748 (2016).
32. Y. Wen, H. Yu, W. Zhao, F. Wang, X. Wang, L. Liu, and W. J. Li, "Photonic nanojet sub-diffraction nano-fabrication with in situ super-resolution imaging," IEEE Trans. Nanotechnol. **18**, 226–233 (2019).
33. B. Yan, L. Yue, J. N. Monks, X. Yang, D. Xiong, C. Jiang, and Z. Wang, "Superlensing plano-convex-microsphere (PCM) lens for direct laser nano marking and beyond," Opt. Lett. **45**, 1168–1171 (2020).
34. H. Zhu, B. Yan, S. Zhou, Z. Wang, and L. Wu, "Synthesis and super-resolution imaging performance of a refractive-index-controllable microsphere superlens," J. Mater. Chem. C **3**, 10907–10915 (2015).
35. Z. Wang, B. Luk'yanchuk, L. Yue, B. Yan, J. Monks, R. Dhama, O. V. Minin, I. V. Minin, S. Huang, and A. Fedyanin, "High order Fano resonances and giant magnetic fields in dielectric microspheres," Sci. Rep. **9**, 20293 (2019).
36. L. Yue, B. Yan, J. N. Monks, R. Dhama, C. Jiang, O. V. Minin, I. V. Minin, and Z. Wang, "Full three-dimensional Poynting vector flow analysis of great field-intensity enhancement in specifically sized spherical-particles," Sci. Rep. **9**, 20224 (2019).
37. Y. M. Song, Y. Xie, V. Malyarchuk, J. Xiao, I. Jung, K. J. Choi, Z. Liu, H. Park, C. Lu, R. H. Kim, and R. Li, "Digital cameras with designs inspired by the arthropod eye," Nature **497**, 95–99 (2013).
38. Z. Li and J. Xiao, "Mechanics and optics of stretchable elastomeric microlens array for artificial compound eye camera," J. Appl. Phys. **117**, 014904 (2015).
39. Z. Li, Y. Wang, and J. Xiao, "Mechanics of bioinspired imaging systems," Theor. Appl. Mech. Lett. **6**, 11–20 (2016).